Plasmonics (2020) 15:263–269
https://doi.org/10.1007/s11468-019-01029-1

Terahertz Selective Emission Enhancement from a Metasurface-Coupled Photoconductive Emitter in Quasi-Near-Field Zone

Zhenyu Zhao[1,2] · Xiaobo Zheng[1] · Zoltan Ollmann[2] · Mozhgan Hayati[2] · Wei Peng[3] · Thomas Feurer[2]

Received: 4 May 2019 / Accepted: 3 September 2019 / Published online: 13 September 2019

Abstract
We present a THz emission enhancement of 41 times at 0.92 THz from a metasurface made of T-shaped resonators excited in a quasi-near-field zone. Such a metasurface has an intrinsic transmission minimum with Q factor of 4 at 1.25 THz under far-field excitation. When this metasurface is coupled onto the backside of a 625-μm-thick photoconductive emitter, the metasurface is below the Fraunhofer distance to the excitation source. As such, one broad enhancement around 0.47 THz and another extremely narrow enhancement at 0.92 THz in the emission spectrum are observed owing to a quasi-near-field excitation. Theoretically, the Q factor of the latter is up to 307, which is limited by the spectral resolution in experiment. The numerical simulations indicate that the T-shaped resonators serve as an array of plasmonic antennas resulting in the aforementioned emission enhancement of THz radiation.

Keywords Metamaterial · Quality factor · Terahertz · Quasi-near-field

Introduction

Terahertz (1 THz = 10^{12} Hz) thin-film sensors exhibit potential applications where conventional THz inspection methods are seriously challenged [1, 2]. The detection or characterization of very thin samples or analytes is one such case that has now inspired a burgeoning branch of THz research [3–5]. The key problem is to enhance the THz detection sensitivity of the thin-film sensors. Compared with other solutions, THz thin-film sensing based on resonant metamaterials represents a promising direction due to its high sensitivity [6]. Generally, metamaterials are made of subwavelength resonators whose frequency response can be tailored according to their shape and size. Therefore, metamaterials can be easily tuned by geometric scaling. Metamaterials offer a high flexibility and are beneficial for a variety of applications. For example, to detect small amounts of sample, resonant metamaterials with sharp resonances are beneficial. Already miniscule frequency shifts create obvious changes in the measured transmission at a particular frequency. In order to further decrease the sample amount needed, it would be beneficial if a detectable frequency shift could be induced by covering a small surface fraction, i.e., a few resonators, rather than the entire array. Therefore, there is continuous interest in developing high-Q metamaterials for thin-film sensors. For split-ring resonators (SRR)–based metamaterials, one finds Q factors at the level of 10 [7]. By changing the length of one arm slightly, the SRRs become asymmetric structures. Then, a "dark" mode, i.e., a Fano resonance, will be excited, which exhibits the reported sharp resonance and Q factors up to 12 [8]. A further modification of the asymmetric SSR leads to an asymmetric D-split resonator for which Q factors up to 27.5 were observed [9]. Irrespective of geometry eventually, the Ohmic damping with its associated non-radiative losses will limit the achievable Q factors. Furthermore, the reported high-Q metamaterials were all excited under far-field conditions. Solving Maxwell's equations for the electric and magnetic fields of a localized oscillating source, such as an antenna, surrounded by a homogeneous material (typically vacuum or air), yields fields that, far away, decay proportional to $1/r$ where r is the distance from the source. These are the radiating fields, and the region

✉ Zhenyu Zhao
zyzhao@shnu.edu.cn

[1] Department of Physics, Shanghai Normal University, Shanghai 200234, China

[2] Institute of Applied Physics, University of Bern, CH-3012 Bern, Switzerland

[3] Shanghai Institute of Microsystem and Information Technology, Chinese Academy of Sciences, Shanghai 200050, China

where r is larger compared with the wavelength is the far field. In this region, fields decrease inversely with distance from the source, resulting in an inverse-square law for the radiated power intensity of THz waves [10]. By contrast, the amplitude of non-propagating near fields decreases more rapidly with distance (with inverse-distance squared or cubed), resulting in relative lack of near-field effects for distances lager than a wavelength. Close to the source, however, these fields can be quite strong and may even be enhanced. Generally, near field effects may be observed for distances shorter than the Fraunhofer distance $r_f = 2nD^2\ \lambda$, with antenna diameter D, wavelength λ, and refractive index n. As long as the metasurface is close to the THz radiation source, that is within the Fraunhofer distance, near fields may give rise to a stronger excitation than far fields, which is suggested to result in a comparatively high-Q factor at the resonant frequency.

In this paper, we demonstrate a quasi-near-field-excited THz metamaterial, which has a very high-Q factor exceeding the bottleneck resulting from radiation loss. Metasurface and emitter are integrated on the two sides of a SI-GaAs wafer, so that the THz source will excite the metasurface within the near field before coupling out to free space.

Experiment

The device is fabricated on a 625 ± 25-μm-thick and <100>-oriented semi-insulating gallium arsenide (SI-GaAs) wafer. The wafer is sliced into a rectangular square of 11 mm × 11 mm. Metasurface and emitter are fabricated on the two sides of this wafer. An image of the photoconductive emitter assembly is shown in Fig. 1a. The H-shaped metal structure is deposited on the SI-GaAs and has a length of 10 mm and a width of 1 mm. The middle line of the H-shaped structure is 10 mm in length with a bowtie area in the center. The gap area of 50 μm × 50 μm is in the center of the bowtie, as shown in Fig. 1b. The metasurface is deposited on the other side of this SI-GaAs wafer via photolithography. Each unit cell is 66.7 μm × 66.7 μm in size and contains a single T-shaped metallic resonator. The horizontal and the vertical strips are 24 μm in length and 4 μm in width, as shown in Fig. 1c, d. The metallic structures (emitter electrodes and metasurface) are made of 120-nm-thick gold (Au) on top of a 5-nm titanium layer (Ti) both of which are deposited on the patterned substrate. The titanium acts as an adhesion layer between Au and SI-GaAs. Regarding the refractive index of SI-GaAs at THz frequencies, i.e., $n = 3.3$, the Fraunhofer distance r_f of our emitter at 1 THz is about 2.2 mm which is larger than the SI-GaAs wafer thickness of 625 ± 25 μm. Therefore, we expect the THz near fields to couple to the metasurface on the opposite side of the wafer. The device assembly is mounted on a home-made adaptor for THz emission measurement. A pair of flexible gold contacts connects to the electrodes of the THz emitter. Figure 1a shows the details of the front side with sample. On the backside, the metasurface is at level with the surface of the mount as shown in Fig. 1c. This ensures that the metasurface is in contact with the high-resistivity spherical silicon lens, which is used for efficient coupling of the THz radiation to the free space part of the setup. The mount sits on a movable 3-axis stage so that

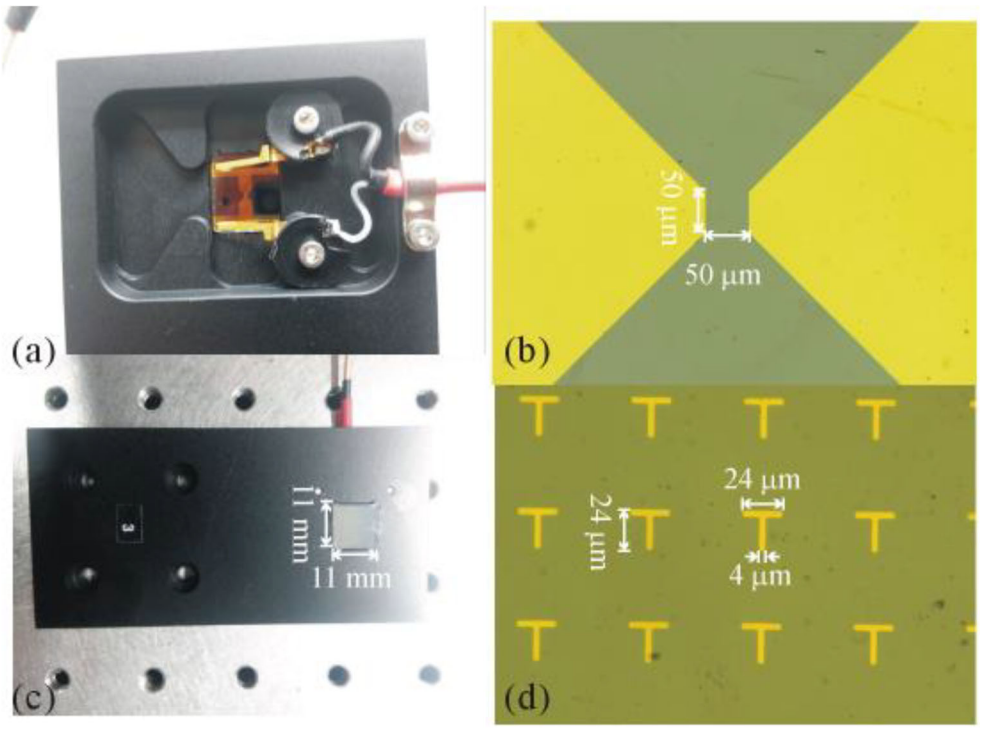

Fig. 1 **a** Front side of the photoconductive antenna. **b** Zoom-in image of the photoconductive antenna; the gap size is 50 μm × 50 μm. **c** Backside of the sample and adaptor; the sample is 11 mm × 11 mm. **d** Microscopic image of T-shaped resonators; the length and width of vertical and horizontal striplines of T-shaped resonator are identical to 24 μm and 4 μm, respectively

the THz output can be optimized manually. Two different samples were fabricated, one of which has no metasurface and is used as a reference.

The THz time-domain spectroscopy experiment (TDS) is based on the pump/probe technique. It uses a femtosecond fiber laser system (Femto Fiber Pro by Toptica) with a pulse duration of 100 fs and a repetition rate of 82 MHz. The average power at a wavelength of 780 nm is 150 mW. The laser beam is divided, via a beamsplitter, into two parts. The stronger pump beam has a maximum power of 100 mW and generates the THz pulses. It is focused on the gap of the photoconductive antenna, which is biased with 80 V from a power supply (WMA-320 Falco System). This voltage is modulated at the frequency of 100 kHz for efficient lock-in detection (HF2 Zurich Instruments). The polarization of the radiated THz wave is across the gap. The weaker part of the beam, with an average power of about 5 mW, is used for electro-optic sampling of the emitted THz pulses. After the beamsplitter, the probe beam is delayed with an electronically controlled, magnetically driven delay stage. It then passes a second beamsplitter and is subsequently guided to a 100-μm-thick <110>-oriented ZnTe detection crystal which, to delay internal reflection, is mounted on a 3-mm-thick sapphire substrate. The ZnTe crystal is coated with a high reflectivity coating from which the probe pulse is reflected back towards the beamsplitter. On its way back through the crystal, it co-propagates with the THz pulse. From the beamsplitter, it is sent through a $\lambda/4$ waveplate and a polarization beamsplitter before a pair of balanced photodiodes measure the two orthogonal polarizations. The signal is filtered, amplified by the lock-in amplifier, and recorded by a computer.

Results and Discussion

The THz emission spectrum of the reference sample (THz emitter without metasurface) is shown in Fig. 2a. The main emission peak is followed by a longer-lasting negative peak (~ 10 ps) superimposed by a rapid oscillation. The relatively long carrier lifetime (~ns level) of SI-GaAs results in slow recombination of the photo-generated carriers. Therefore, the spectral bandwidth is limited to about 1.5 THz with a dynamic range of 30 dB as shown in Fig. 2b. Figure 2c shows the THz waveform of the proposed device (THz emitter with metasurface on the backside). Obviously, the fast oscillations have almost disappeared and the first replica appears more pronounced. Since the metasurface is made of metallic structures, which reflects part of the THz radiation, the maximum output is slightly lower than the THz emission from reference sample. Moreover, the antenna electrodes together with the metasurface form a Fabry-Perot cavity, which leads to the observed replica.

The relative transmission spectrum is calculated from the Fourier transforms of the time-domain electric fields [11]:

$$T = E_{\text{sample}}(\nu)/E_{\text{ref}}(\nu), \tag{1}$$

where $E_{\text{sample}}(\nu)$ and $E_{\text{ref}}(\nu)$ are the electric fields measured after the metasurface-coupled THz antenna and the THz antenna without metasurface, respectively. The transmission as a function of frequency is shown in Fig. 3 and we observe several prominent features. The average transmission is about 0.65 and it is superimposed by a periodic oscillation due to the aforementioned Fabry-Perot cavity. Moreover, we find an unexpected narrow spectral peak at around 0.92 THz and a much broader feature peaked at around 0.47 THz. The maximum transmission of the narrow peak indicates a twice as high THz output compared with the reference emitter. This extraordinary increase in transmission is fundamentally different from the far-field resonance of the metasurface. In fact, most metamaterials made of positive metal structures, such as split-ring resonators [11–13], cut wires [14, 15], or U-shaped resonators [16, 17], exhibit a decrease in transmission at the resonance frequencies. Only negative structures, i.e., complementary structures, show a transmission enhancement [18, 19]. In our case, a zoom of the far-field transmission of the metasurface is

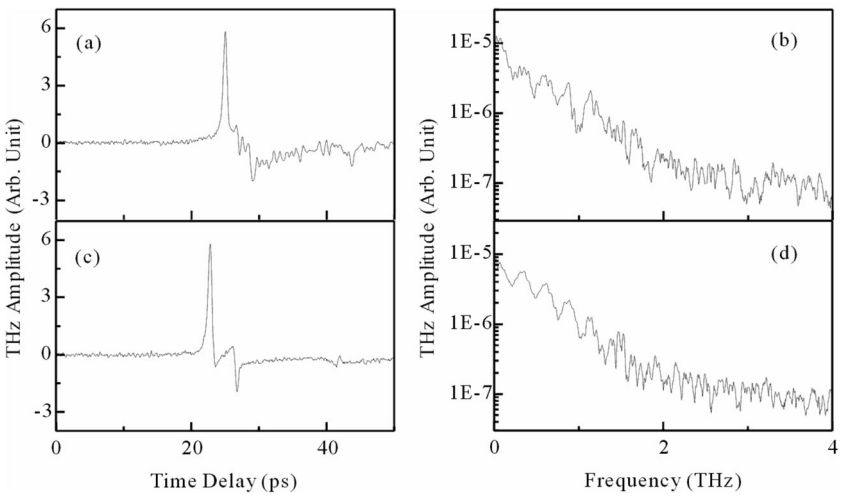

Fig. 2 **a** THz waveform of emitter without metasurface. **b** THz spectrum of emitter without metasurface. **c** THz waveform of emitter with metasurface. **d** THz spectrum of emitter with metasurface

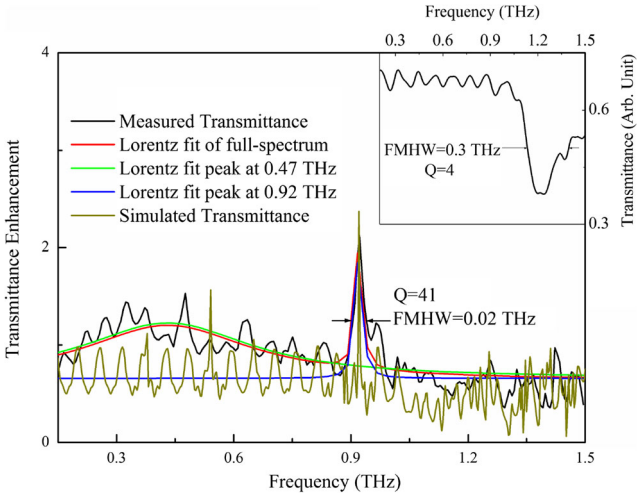

Fig. 3 Dark-green solid line, the simulated transmission spectrum. Black solid line, the retrieved transmission spectrum. Blue solid line, Lorentz fit to resonance mode at 0.92 THz. Green solid line, Lorentz fit to resonance mode at 0.45 THz. Red solid line, multi-peak Lorentz fit of the entire transmission spectrum. Inset, simulated THz response of T-shaped metasurface excited under far-field condition

illustrated in the inset of Fig. 3 and shows a broad spectral dip at around 1.25 THz. Its Q factor is only about 4, which is derived from [19].

$$Q = \nu/\Delta\nu \tag{2}$$

Here, ν is the central frequency of resonance, and $\Delta\nu$ is the full width at half maximum (FWHM). The same far-field resonance is not observed under near-field excitation. On the contrary, an unforeseen extraordinary transmission enhancement at 0.47 THz and 0.92 THz is recorded.

In order to reveal the origin of the aforementioned extraordinary transmission enhancement, we simulate the geometry with the CST Microwave Studio™ software in three spatial dimensions. Specifically, we analyze surface currents and electromagnetic field distributions. Due to memory limitations, the simulations are restricted to a 4×4 unit cell area of the metasurface, which is much smaller than the entire metasurface with 150×150 unit cells. Therefore, scattering effects in between unit cells of the metasurface are suppressed, which makes the simulated resonance linewidths narrower than for the entire metasurface.

Figure 4a shows the surface current loop of the broadband mode at 0.47 THz. The current on the horizontal strip is higher than that on the vertical strip of each individual T-shaped resonator. Analyzing the corresponding electric field distribution, shown in Fig. 4b, reveals that only four resonators in the center, i.e., just on top of the antenna structure, are activated by the quasi-near-field excitation. While the positive charges accumulate on the right two resonators, the negative charges accumulate on the left two resonators. That is, the T-shaped resonators act as electrodes of an equivalent short dipole antenna as indicated in Fig. 4b. Meanwhile, the gap areas in between the adjacent T-shaped resonators act as feed point impedances. The resonance linewidth of a short dipole antenna is defined as the ratio of the inductor or the capacitor reactance to the resistance [20]. A long gap means a large capacitor reactance compared with the resistance so that the resonance linewidth of the 0.47-THz mode becomes very broad. Finally, Fig. 4c shows the electrical field distribution in the GaAs wafer along the direction of the wavevector. Due to the Fraunhofer diffraction from the photoconductive antenna, a series of wave maxima and minima propagate along the z-axis. The dimensions of the central band are related to the gap area of the photoconductive antenna, as shown at the left boundary of Fig. 4c. The large off-resonance reactance in combination with diffraction effect results in the broadband and relatively weak extraordinary transmission at 0.47 THz. Fitting the measured resonance at 0.92 THz to a Lorentz model reveals a linewidth of 20 GHz, which is identical to the spectral resolution of our TDS setup. Thus, the true linewidth may be even smaller and the deduced Q factor of 41 is only a lower limit. For comparison, the simulated Q factor is 307. It is well known that the Q factor of metallic metamaterials is limited to below 10 due to non-radiative losses [7]. If one wants to achieve higher Q factors, a dark Fano resonance needs to be excited which occurs only in asymmetric geometries [21, 22]. Since the T-shaped resonators used here are symmetric, a Fano resonance as the origin of the sharp mode at 0.92 THz can be excluded. Figure 5 summarizes the simulation results with respect to the narrow mode at 0.92 THz. At this frequency, the surface currents on the metasurface (Fig. 5a) indicate a mono-directional current flow along the horizontal strips of T-shaped resonators. Also, the currents on vertical strips are in horizontal direction but much weaker than the currents on horizontal strips. Consequently, only the horizontal strips are activated by quasi-near-field excitation. Figure 5b shows the electric field distribution at the interface between SI-GaAs and the metasurface. The dipolar charges accumulate at the left and right terminals of the T-shaped resonators which is indicative for a surface plasmon dipole oscillation. The surface plasmons propagating along the metal GaAs interface are a manifestation of an electron density wave, which is driven by the radiated electric field of the THz wave. Their propagation direction must be along the direction of THz polarization at normal incidence [23, 24], which here is parallel to the horizontal strip of the T-shaped resonators. The vertical strip of T-shaped resonators is unable to support surface plasmon oscillations, which is in agreement with the simulated surface currents shown in Fig. 5a. According to previous

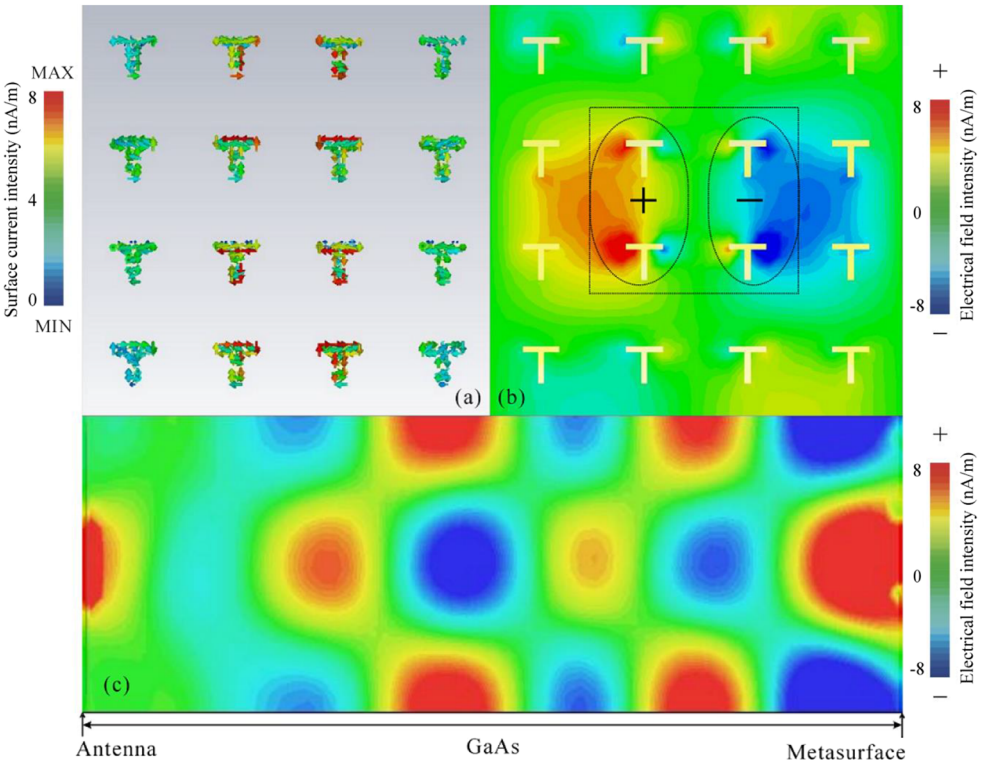

Fig. 4 Resonance mode at 0.47 THz: Surface currents (**a**) and electric field distribution (**b**) in the metasurface. The ellipses indicate the equivalent short dipole antenna and the rectangular dash line box the equivalent feed line of the dipole antenna. **c** Electric field distribution inside the GaAs substrate (*xz*-plane). The THz radiation propagates from left to right. The color bar refers to the strength of surface current and electric field correspondingly

works [25, 26], a dipole oscillation in metallic resonators should give rise to an absorption feature in the THz transmission spectrum. Conversely, here we observe the opposite behavior, namely an emission enhancement that we hereafter explain on the basis of electromagnetic field simulations. Figure 5c depicts the electric field inside the SI-GaAs wafer with the main propagation direction along the *z*-axis at the resonance wavelength of

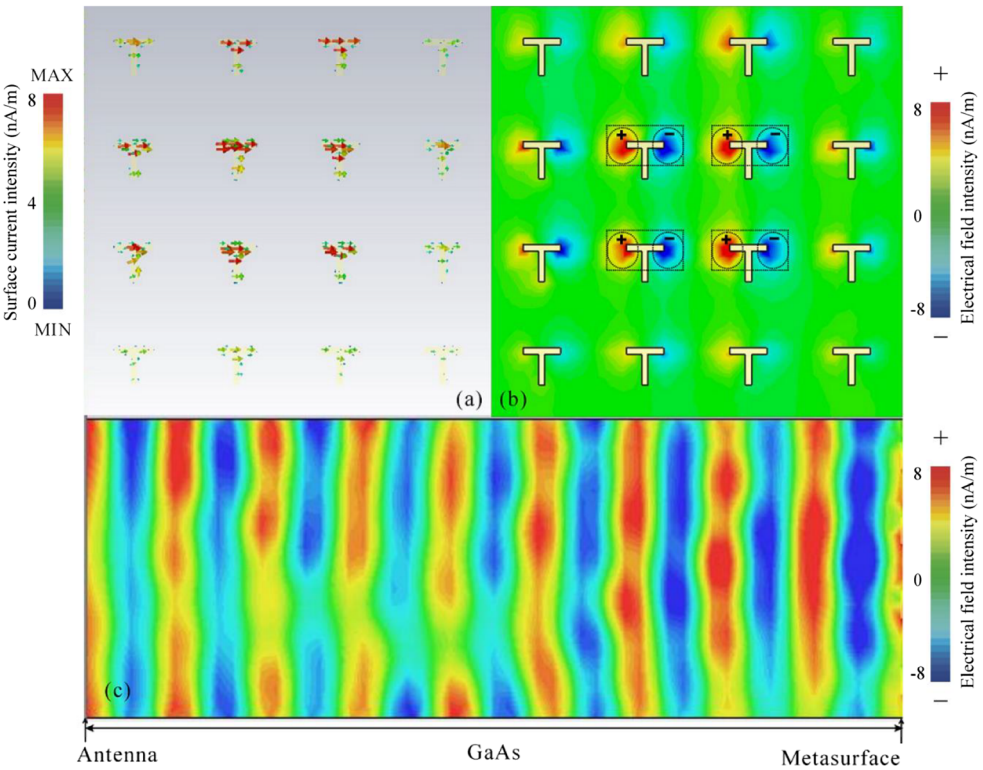

Fig. 5 Resonance mode at 0.92 THz: Surface currents (**a**) and electric field distribution (**b**) in the metasurface (*xy*-plane). The circular area in dash line, the pole of antenna; the rectangular area in dash line, the equivalent plasmonic antenna. **c** Electric field distribution inside the GaAs substrate (*xz*-plane). The THz radiation propagates from left to right. The color bar refers to the strength of the surface current and electric field correspondingly

0.92 THz. When the THz wave arrives at the metasurface, most of radiation is diffracted to free space via the four T-shaped resonators closest to the gap of the photoconductive antenna. Part of the energy accumulates in the regions between two adjacent T-shaped resonators. It is known that the non-radiative electromagnetic field trapped in regions close to the source is not drawing any power from the emitter unless it excites another object close to it. Here, the T-shaped resonators can be excited by the non-radiative electromagnetic near field, in which case the horizontal strip of T-shaped resonator plays the role of a plasmonic antenna as shown in Fig. 5b. Thus, the whole metasurface becomes an array of plasmonic antennas forming an interface between the localized radiation emitter and free space. In transmission mode, they have the ability to direct and enhance the radiative emission [27–29]. Therefore, the high-Q factor at 0.92 THz is a result of the plasmonic antenna gain excited by the quasi-near-field excitation, which emits to free space. It generally only performs optimally over a rather narrow bandwidth. Thus, we conclude that the metasurface of T-shaped resonators acts as an array of plasmonic antennas excited by the near field of the emitter, which results in the emission enhancement and the high-Q factor at 0.92 THz. According to the principle of near-field behavior of plasmonics, the enhancement factor relies on the distance between the object and radiation source [30–32]. Herein, we address that our result of enhancement is limited by the SI-GaAs substrate thickness of 625 μm. A higher enhancement factor may be achieved with the SI-GaAs substrate thickness reduced to nanometer level.

Conclusion

In summary, the THz response of a metasurface excited under near-field conditions has been investigated experimentally. The hybrid device consisted of a semi-insulating gallium arsenide wafer with a THz photoconductive antenna on one side and a metasurface of T-shaped resonators on the other side. The thickness of SI-GaAs was 625 μm; that is, the metasurface was within the range of the near field of the emitter. The simulated far-field resonance of the metasurface was at 1.25 THz with a Q factor of 4, but was unseen under near-field excitation condition. On the contrary, an extraordinary transmission enhancement at around 0.92 THz was observed. Its maximum transmission was twice higher than that of the photoconductive antenna without metasurface. Moreover, its Q factor was as high as 41, which exceeded the Q factor of the metasurface excited by far-field THz radiation. With the help of electromagnetic simulations, we attributed this behavior to a surface plasmon dipole oscillation along the horizontal strips of the T-shaped resonators, which drew its energy from the near field of the THz emitter and subsequently radiated into free space. The emission was within a very narrow frequency range resulting in a high-Q factor.

Acknowledgments The authors acknowledge the contribution of Matthias Ulrich and Niklaus Jaussi for sample fabrication.

Funding information This work is financially supported by the Joint Research Fund in Astronomy (U1631112) under the cooperative agreement between the National Natural Science Foundation of China (NSFC) and Chinese Academy of Sciences (CAS), and the Swiss National Science Foundation (SNSF# 200020_165686). Zhenyu Zhao acknowledges the Swiss National Science Foundation International Short Visit Program (IZK0Z2_173458).

References

1. Tonouchi M (2007) Cutting-edge terahertz technology. Nat Photonics 1:97–105
2. Park SJ, Hong JT, Choi SJ, Kim HS, Park WK, Han ST, Park YJ, Lee S, Kim DS, Ahn YH (2014) Detection of microorganisms using terahertz metamaterials. Sci Rep 4:4988-1-7
3. Zheludev NI, Kivshar YS (2012) From metamaterials to metadevices. Nat Mater 11:917–924
4. Bogomazova AN, Vassina EM, Goryachkovskaya TN, Popik VM, Sokolov AS, Kolchanov NA, Lagarkova MA, Kiselev SL, Peltek SE (2015) No DNA damage response and negligible genome-wide transcriptional changes in human embryonic stem cells exposed to terahertz radiation. Sci Rep 5:7749-4-6
5. Zibik EA, Grange T, Carpenter BA, Porter NE, Ferreira R, Bastard G, Stehr D, Winnerl S, Helm M, Liu HY, Skolnick MS, Wilson LR (2009) Long lifetimes of quantum-dot intersublevel transitions in the terahertz range. Nat Mater 8:803–807
6. Woltman SJ, Jay GD, Crawford GP (2007) Liquid-crystal materials find a new order in biomedical applications. Nat Mater 6:929–938
7. Luk'yanchuk B, Zheludev NI, Maier SA, Halas NJ, Nordlander P, Giessen H, Chong CT (2010) The Fano resonance in plasmonic nanostructures and metamaterials. Nat Mater 9:707–715
8. Fedotov VA, Rose M, Prosvirnin SL, Papasimakis N, Zheludev NI (2007) Sharp trapped-mode resonances in planar metamaterials with a broken structural symmetry. Phys Rev Lett 99:147401–1-4
9. Jansen C, Al-Naib IAI, Born N, Koch M (2011) Terahertz metasurfaces with high Q-factors. Appl Phys Lett 98:051109–1-4
10. Kawano Y, Ishibashi K (2008) An on-chip near-field terahertz probe and detector. Nat Photonics 2:618–621
11. Cao W, Singh R, Zhang C, Han J, Tonouchi M, Zhang W (2013) Plasmon-induced transparency in metamaterials: active near field coupling between bright superconducting and dark metallic mode resonators. Appl Phys Lett 103:101106–1-5
12. Hokmabadi MP, Philip E, Rivera E, Kung P, Kim SM (2015) Plasmon-induced transparency by hybridizing concentric-twisted double split ring resonators. Sci Rep 5:15735–1-11
13. Merbold H, Bitzer A, Feurer T (2011) Near-field investigation of induced transparency in similarly oriented double split-ring resonators. Opt Lett 36:1683–1685
14. Liu N, Weiss T, Mesch M, Langguth L, Eigenthaler U, Hirscher M, Sönnichsen C, Giessen H (2010) Planar metamaterial analogue of electromagnetically induced transparency for plasmonic sensing. Nano Lett 10:1103–1107
15. Duan X, Chen S, Yang H, Cheng H, Li J, Liu W, Gu C, Tian J (2012) Polarization-insensitive and wide-angle plasmonically

induced transparency by planar metamaterials. Appl Phys Lett 101: 143105–1-04
16. Li Z, Ma Y, Huang R, Singh R, Gu J, Tian Z, Han J, Zhang W (2011) Manipulating the plasmon-induced transparency in terahertz metamaterials. Opt Express 19:8912–8919
17. Wan M, Song Y, Zhang L, Zhou F (2015) Broadband plasmon-induced transparency in terahertz metamaterials via constructive interference of electric and magnetic couplings. Opt Express 23: 27361–27368
18. Chen HT, O'Hara JF, Taylor AJ, Averitt RD, Highstrete C, Lee M, Padilla WJ (2007) Complementary planar terahertz metamaterials. Opt Express 15:1084–1095
19. Song Z, Zhao Z, Zhao H, Peng W, He X, Shi W (2015) Teeter-totter effect of terahertz dual modes in C-shaped complementary split-ring resonators. J Appl Phys 118:043108–1-6
20. Warren S, Gary T (1981) Antenna Theory And Design. Wiley
21. Singh R, Al-Naib IAI, Yang Y, Chowdhury DR, Cao W, Rockstuhl C, Ozaki T, Morandotti R, Zhang W (2011) Observing metamaterial induced transparency in individual Fano resonators with broken symmetry. Appl Phys Lett 99:201107–1-4
22. Zhang F, Huang XC, Zhao Q, Chen L, Wang Y, Li Q, He X, Li C, Chen K (2014) Fano resonance of an asymmetric dielectric wire pair. Appl Phys Lett 105:172901–1-4
23. Degl'Innocenti R, Jessop DS, Sol CWO, Xiao L, Kindness SJ, Lin H, Zeitler JA, Braeuninger-Weimer P, Hofmann S, Ren Y, Kamboj VS, Griffiths JP, Beere HE, Ritchie DA (2016) Fast modulation of terahertz quantum cascade lasers using graphene loaded plasmonic antennas. ACS Photonics 3:464–470
24. Giannini V, Fernandez-Domínguez AI, Heck SC, Maier SA (2011) Plasmonic nanoantennas: fundamentals and their use in controlling the radiative properties of nanoemitters. Chem Rev 111:3888–3912
25. Zhao Z, Zheng X, Peng W, Zhang J, Zhao H, Shi W (2017) Localized terahertz electromagnetically-induced transparency-like phenomenon in a conductively coupled trimer metamolecule. Opt Express 25:24410–24424
26. Zhao Z, Zheng X, Peng W, Zhao H, Zhang J, Luo Z, Shi W (2017) Localized slow light phenomenon in symmetry broken terahertz metamolecule made of conductively coupled dark resonators. Opt Mater Express 7:1950–1961
27. Neubrech F, Huck C, Weber K, Pucci A, Giessen H (2017) Surface-enhanced infrared spectroscopy using resonant nanoantennas. Chem Rev 117:5110–5145
28. Coenen T, Vesseur EJR, Polman A (2012) Deep subwavelength spatial characterization of angular emission from single-crystal Au plasmonic ridge nanoantennas. ACS Nano 6:1742–1750
29. Flauraud V, Regmi R, Winkler PM, Alexander DTL, Rigneault H, van Hulst NF, García-Parajo MF, Wenger J, Brugger J (2017) In-plane plasmonic antenna arrays with surface nanogaps for giant fluorescence enhancement. Nano Lett 17:1703–1710
30. Kawata S, Inouye Y, Verma P (2009) Plasmonics for near-field nano-imaging and superlensing. Nat Photonics 3:388–394
31. Ciracì C, Hill RT, Mock JJ, Urzhumov Y, Fernández-Domínguez AI, Maier SA, Pendry JB, Chilkoti A, Smith DR (2012) Probing the ultimate limits of plasmonic enhancement. Science 337:1072–1074
32. Malakoutian M, Byambadorj T, Davaji B, Richie J, Lee CH (2017) Optimization of the bowtie gap geometry for a maximum electric field enhancement. Plasmonics 12:287–292